UNIVERSITI TEKNOLOGI MARA
MATHEMATICS LETTERS
https://sites.google.com/tmsk.uitm.edu.my/mathematicsletters

Magnetohydrodynamic (MHD) Flow of A Nanofluid Over a Stretching Surface with Suction and Slip Effects

[1]Nurul Faqihah Azmi & [2,*] Nadhirah Abdul Halim
[1&2]School of Mathematical Sciences, Faculty of Computer and Mathematical Sciences, Universiti Teknologi MARA
[1]2023305793@student.uitm.edu.my
[*2] nadhirahhalim@uitm.edu.my
*Corresponding author

Received: 11/3/2026 Revised: 31/3/2026 Accepted: 5/4/2026 Published: 30/4/2026

ABSTRACT

Magnetohydrodynamic (MHD) nanofluid flow over stretching surfaces plays an important role in many thermal engineering applications, particularly in systems where enhanced heat transfer and flow control are required. This study examines the influence of magnetic field, suction, velocity slip, velocity ratio, and nanoparticle volume fraction on the flow and heat transfer characteristics of nanofluids over a stretching surface. Three types of nanoparticles are considered, namely copper (Cu), aluminium oxide (Al_2O_3), and titanium oxide (TiO_2). The governing nonlinear partial differential equations representing the conservation of mass, momentum, and energy are transformed into a system of ordinary differential equations using similarity transformations. The resulting equations are solved numerically using the bvp4c solver in MATLAB. The numerical results show that the magnetic field and suction parameters enhance both the skin friction coefficient and the local Nusselt number, indicating stronger wall shear and improved heat transfer. Increasing the nanoparticle volume fraction improves the thermal performance of the fluid due to higher effective thermal conductivity, although excessive concentration increases viscosity and affects the velocity distribution. Among the nanofluids considered, Cu provides the highest heat transfer performance, while Al_2O_3 offers a more practical balance between thermal efficiency, stability, and cost. These findings highlight the potential of MHD nanofluids with slip and suction effects for improving thermal management in engineering and industrial heat transfer systems.

Keywords: Heat Transfer, MHD Flow, Nanofluid, Suction, Slip Velocity

INTRODUCTION

Efficient heat transfer is essential in engineering applications, including electronic cooling, energy systems, and material processing. Conventional fluids such as water, oil, and ethylene glycol are limited by their low thermal conductivity. Nanofluids, created by dispersing nanoparticles (1–100 nm) into a base fluid, offer enhanced thermal performance. Choi and Eastman (1995) first showed that metallic nanoparticles improve thermal conductivity, while subsequent studies confirmed their practical benefits. For instance, Safie et al. (2020) examined Al_2O_3 nanofluid stability, Zheng et al. (2020)

reported improved heat transfer in double-tube exchangers, Karimdoost and Soleimani (2021) demonstrated enhanced radiator performance with tube inserts, and Hussein et al. (2025) highlighted the effect of nanoparticle concentration on heat transfer in coils.

Nanofluid flows can be further influenced by magnetohydrodynamics (MHD), governing electrically conducting fluids under magnetic fields. MHD enables control over fluid velocity and temperature, critical for thermal management. Early investigations such as Othman et al. (2021) studied carbon nanotube nanofluids and reported that magnetic parameters enhance skin friction and heat transfer. Zhang et al. (2021) highlighted the role of Joule heating in controlling fluid motion, while Khan and Nadeem (2021) examined mass and heat transfer in Maxwell nanofluids, showing complex flow behaviour under magnetic fields. More recently, Alabdulhadi et al. (2023) demonstrated that Brownian motion influences heat and mass transfer in MHD nanofluid flow over moving surfaces with suction, and Oyekunle et al. (2024) showed that magnetic fields enhance momentum and modify thermal distribution in porous media. Collectively, these studies emphasize the importance of magnetic effects on nanofluid boundary layer behaviour.

In practical systems, nanofluid flows often occur over stretching surfaces, such as in polymer extrusion, glass fibre production, and metal forming. Suction can stabilize the boundary layer, reduce thickness, and improve heat transfer. Earlier studies (Khashi'ie et al., 2022; Zainal et al., 2022; Khan et al., 2022) showed that suction enhances thermal performance and skin friction. More recent works (Emam et al., 2025; Alias et al., 2025) confirmed that suction significantly improves heat transfer in nanofluid flows, highlighting its practical relevance for industrial applications.

Another important factor is velocity slip at the surface, which occurs in micro- and nanoscale systems where the no-slip condition does not hold. Slip modifies the boundary layer and influences both momentum and heat transfer. Studies have demonstrated that slip affects velocity and thermal distributions in MHD nanofluids (Jagadish and Tawade, 2022; Japili et al., 2022; Nor et al., 2022; Naqvi et al., 2022; Joyce et al., 2023).

Although nanofluid flow, MHD effects, suction, and slip have been investigated extensively, many studies focus on these mechanisms separately or under simplified conditions. A comprehensive analysis combining magnetic fields, suction, and velocity slip over stretching surfaces remains limited. This study addresses this gap by modelling and analysing MHD nanofluid flow with suction and slip, incorporating insights from recent 2025 studies, to guide the design of efficient heat transfer systems and boundary layer control in electronic cooling, energy, and manufacturing applications.

THE MATHEMATICAL MODEL

This study considers a steady, two-dimensional, incompressible nanofluid flow in the region $y > 0$ over a permeable stretching surface at $y = 0$, influenced by a magnetic field B_0 and velocity slip (Figure 1). The surface stretches linearly with velocity $U_w(x) = ax$, while the ambient fluid moves with $U_\infty(x) = bx$, where a and b are positive constants.

Figure 1

Physical model of stagnation point flow over a stretching surface

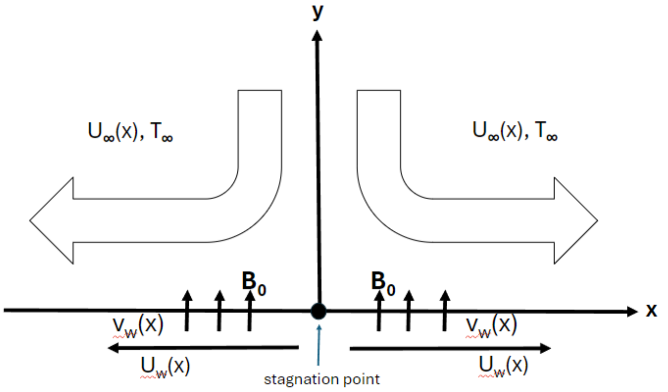

The flow is governed by the boundary layer equations for mass, momentum, and energy:

.

$$\frac{\partial u}{\partial x} + \frac{\partial v}{\partial y} = 0 \tag{1}$$

$$u\frac{\partial u}{\partial x} + v\frac{\partial u}{\partial y} = U_\infty \frac{\partial U_\infty}{\partial x} + \frac{\mu_{nf}}{\rho_{nf}}\frac{\partial^2 u}{\partial y^2} + \frac{\sigma B_0^2}{\rho_{nf}}(U_\infty - u) \tag{2}$$

$$u\frac{\partial T}{\partial x} + v\frac{\partial T}{\partial y} = \alpha_{nf}\frac{\partial^2 T}{\partial y^2} \tag{3}$$

with boundary conditions:

$$\begin{aligned} &u = U_w(x) + L\left(\frac{\partial u}{\partial y}\right), \quad v = v_w(x), \quad T = T_w \quad &&\text{at } y = 0 \\ &u \to U_\infty(x), \quad T \to T_\infty &&\text{as } y \to \infty \end{aligned} \tag{4}$$

Here, $\boldsymbol{u}$ and $\boldsymbol{v}$ are velocity components along $\boldsymbol{x}$ and $\boldsymbol{y}$; $\boldsymbol{T}$ is the nanofluid temperature; $\boldsymbol{L}$ is the slip length; $\boldsymbol{v_w}$ is the suction velocity; $\boldsymbol{\sigma}$ is electrical conductivity; and $\boldsymbol{\mu_{nf}}$, $\boldsymbol{\alpha_{nf}}$, $\boldsymbol{\rho_{nf}}$ are nanofluid viscosity, thermal diffusivity, and density, respectively.

Three types of nanoparticles are considered: Copper (Cu), Aluminium Oxide (Al_2O_3), and Titanium Oxide (TiO_2) in a water-based nanofluid. The thermophysical properties of the base fluid and nanoparticles are listed in Table 1, and the nanofluid properties are defined by Mahmood et al. (2022) in Table 2 below:

Table 1

Thermophysical properties of nanoparticles and base fluid. (Yashkun et al. 2020)

Physical Properties	**Base Fluid (water)**	$\boldsymbol{TiO_2}$	$\boldsymbol{Al_2O_3}$	$\boldsymbol{Cu}$
$\boldsymbol{\rho\left(\frac{kg}{m^3}\right)}$	997.1	4250	3970	8933

$C_p\left(\frac{J}{kgK}\right)$	4179	686.2	765	385
$k\left(\frac{W}{mK}\right)$	0.613	8.9538	40	400

Table 2

Nanofluids thermophysical properties. (Mahmood et al. 2022)

Thermophysical properties	Equation	
Viscosity	$\mu_{nf} = \frac{\mu_f}{(1-\varphi)^{2.5}}$	(5)
Thermal diffusivity	$\alpha_{nf} = \frac{k_{nf}}{(\rho C_p)_{nf}}$	(6)
Density	$\rho_{nf} = (1-\varphi)\rho_f + \varphi\rho_s$	(7)
Heat capacity	$(\rho C_p)_{nf} = (1-\varphi)(\rho C_p)_f + \varphi(\rho C_p)_s$	(8)
Thermal conductivity	$\frac{k_{nf}}{k_f} = \frac{(k_s+2k_f)-2\varphi(k_f-k_s)}{(k_s+2k_f)+\varphi(k_f-k_s)}$	(9)

where φ is the nanoparticle volume fraction, with $0 \le \varphi \le 0.2$, k_{nf} is the nanofluid thermal conductivity and $(\rho C_p)_{nf}$ is the nanofluid heat capacity. ρ_f and ρ_s are the densities of the fluid and solid fraction, k_f and k_s are the thermal conductivities of fluid and solid fractions.

THE SIMILARITY TRANSFORMATION

To reduce the partial differential equations (PDEs) to ordinary differential equations (ODEs), the similarity variable $\boldsymbol{\eta}$, stream function $\boldsymbol{\psi}$, and dimensionless temperature $\boldsymbol{\theta}$ are defined as:

$$\eta = \left(\frac{b}{v_f}\right)^{\frac{1}{2}} y, \qquad \psi = (v_f b)^{\frac{1}{2}} x f(\eta), \qquad \theta(\eta) = \frac{T - T_\infty}{T_w - T_\infty} \tag{10}$$

where $v_f = \frac{\mu_f}{\rho_f}$ is the fluid kinematic viscosity, T_w is the fluid temperature at the stretching surface while T_∞ is the ambient temperature.

The velocity components are represented as $u = \partial\psi/\partial y$ and $v = -\partial\psi/\partial x$, which satisfy the continuity equation automatically. Substituting Equation 10 into the momentum and energy equations gives:

$$\frac{1}{(1-\varphi)^{2.5}\left(1-\varphi+\varphi\frac{\rho_s}{\rho_f}\right)}f'''+ff''-f'^2+1+M(1-f')=0 \quad (11)$$

$$\frac{1}{Pr}\frac{k_{nf}/k_f}{\left[(1-\varphi)+\varphi\left(\rho C_p\right)_s/\left(\rho C_p\right)_f\right]}\theta''+f\theta'=0 \quad (12)$$

with boundary conditions:

$$\begin{array}{llll} f(0)=\gamma, & f'(0)=\lambda+\delta f''(0), & \theta(0)=1 & \text{at } \eta=0 \\ f'(0)\to 1, & \theta(\eta)\to 0 & & \text{as } \eta\to\infty \end{array} \quad (13)$$

where $\boldsymbol{M=\sigma B_0^2/(\rho_f b)}$is the magnetic parameter, $\boldsymbol{Pr=\nu_f/\alpha}$is the Prandtl number, $\boldsymbol{\lambda=b/a}$ is the velocity ratio, $\boldsymbol{\gamma=v_w/\sqrt{\nu_f b}}$ is the suction parameter, and $\boldsymbol{\delta=L\sqrt{b/\nu_f}}$ is the slip parameter.

The skin friction coefficient, C_f and the local Nusselt number, Nu_x are defined as:

$$C_f=\frac{\tau_w}{\rho_f {U_\infty}^2}, \qquad Nu_x=\frac{xq_w}{k_f(T_w-T_\infty)} \quad (14)$$

where τ_w is the surface shear stress along the plate and q_w is the heat flux from the plate.

$$\tau_w=\mu_{nf}\left(\frac{\partial u}{\partial y}\right)_{y=0}, \qquad q_w=-k_{nf}\left(\frac{\partial T}{\partial y}\right)_{y=0} \quad (15)$$

Using similarity transformations, these reduce to:

$$C_f Re_x^{1/2}=\frac{1}{(1-\varphi)^{2.5}}f''(0) \quad (16)$$

$$\frac{Nu_x}{Re_x^{1/2}}=-\left(\frac{k_{nf}}{k_f}\right)\theta'(0) \quad (17)$$

where $Re_x^{1/2}=\frac{U_\infty x}{v_f}$ is the local Reynolds number.

THE NUMERICAL SOLUTION

The transformed ordinary differential equations (11) and (12), subject to boundary conditions (13), are solved numerically using MATLAB's bvp4c solver. This solver is specifically designed for boundary value problems (BVPs) of ODEs and provides robust solutions for nonlinear and coupled systems.

The governing ODEs are first rewritten in first-order form to conform to bvp4c requirements. The shooting method is not used, as bvp4c directly handles the boundary conditions at both ends of the domain. The infinity boundary is approximated numerically by setting $\eta_\infty=20$, which ensures that $f'(\eta_\infty)$and $\theta(\eta_\infty)$effectively reach their asymptotic values.

The solver iteratively adjusts the solution to satisfy the boundary conditions with a tolerance of 10^{-6}. The effects of key parameters, including the magnetic parameter M, suction parameter γ, slip parameter δ, velocity ratio λ, and nanoparticle volume fraction ϕ, are examined by varying one parameter at a time while keeping others constant.

The skin friction coefficient C_f and local Nusselt number Nu_x are calculated from the numerical solutions of $f''(0)$ and $\theta'(0)$ using equations (16) and (17). Velocity and temperature profiles are plotted for different parameter values to analyse boundary layer behaviour, flow control, and heat transfer characteristics.

To ensure accuracy and reliability, the numerical method is validated against the reference results for the skin friction coefficient $C_f Re_x^{1/2}$ and the local Nusselt number $Nu_x/Re_x^{1/2}$ reported by Yashkun et al. (2020). Tables 3 and 4 summarize the comparison for different values of the velocity ratio parameter λ and nanoparticle volume fraction ϕ, while keeping the slip parameter $\delta = 0$ and suction parameter $\gamma = 0$, with Prandtl number $Pr = 6.2$.

Table 3

Comparison value of the skin friction coefficient

λ	φ	Yashkun et al. (2020)			Present results		
		Cu	Al_2O_3	TiO_2	Cu	Al_2O_3	TiO_2
0	0.1	1.884324	1.602057	1.619292	1.88432	1.60206	1.61929
	0.2	2.622743	2.058324	2.094220	2.62274	2.05832	2.09422
0.3	0.1	1.447449	1.230625	1.243864	1.44745	1.23062	1.24386
	0.2	2.014668	1.581109	1.608682	2.01467	1.58111	1.60868
0.5	0.1	1.090453	0.927106	0.937079	1.09045	0.92711	0.93708
	0.2	1.517774	1.191147	1.211919	1.51777	1.19115	1.21192

Table 4

Comparison value of the local Nusselt number

λ	φ	Yashkun et al. (2020)			Present results		
		Cu	Al_2O_3	TiO_2	Cu	Al_2O_3	TiO_2
0	0.1	1.404327	1.330508	1.301085	1.40433	1.33051	1.30108
	0.2	1.669338	1.535160	1.469033	1.66934	1.53516	1.46903
0.3	0.1	1.694789	1.639754	1.604959	1.69479	1.63975	1.60496
	0.2	1.971910	1.867288	1.790581	1.97191	1.86729	1.79058
0.5	0.1	1.872386	1.827847	1.789738	1.87239	1.82785	1.78974
	0.2	2.157690	2.069987	1.986723	2.15769	2.06999	1.98672

The comparison shows excellent agreement between the present study and the reference values, with deviations less than 1% in all cases. This confirms the accuracy and reliability of the numerical procedure, including the similarity transformation, boundary approximation, and MATLAB bvp4c solver. Therefore, the method is considered valid for the full analysis involving magnetic field, suction, slip, and nanoparticle effects.

RESULTS AND DISCUSSION

This section presents the numerical results for the MHD nanofluid flow over a stretching surface, considering the effects of the magnetic field M, suction γ, velocity slip δ, velocity ratio λ, and nanoparticle volume fraction ϕ on the skin friction coefficient, local Nusselt number, and the velocity and temperature profiles. The baseline parameter values used throughout the analysis are $\Pr = 6.2$, $\varphi = 0.1$, $\lambda = 0.5$, $M = 0.3$, $\delta = 1$ and $\gamma = 1$, unless stated otherwise.

Effect on Skin Friction Coefficient, $C_f Re_x^{\frac{1}{2}}$

Table 5 shows that Cu nanofluid exhibits a higher skin friction coefficient compared to Al_2O_3 and TiO_2 nanofluids. This is primarily due to the higher density of Cu nanoparticles, which increases the overall density and effective viscosity of the nanofluid. As a result, the fluid near the wall experiences greater resistance, producing higher wall shear stress and an increased skin friction coefficient.

Table 5

Values of $C_f Re_x^{\frac{1}{2}}$ *for various values of the parameter*

Variables					Nanoparticles		
λ	φ	M	δ	γ	Cu	Al_2O_3	TiO_2
0					0.95413	0.89491	0.89893
0.5	0.1	0.3	1	1	0.47911	0.45032	0.45227
1					0.00000	0.00000	0.00000
1.5					-0.48282	-0.45542	-0.45727
0.5	0				0.34622	0.34622	0.34622
	0.05	0.3	1	1	0.40978	0.39444	0.39540
	0.1				0.47911	0.45032	0.45227
	0.2				0.65143	0.59368	0.59797
0.5	0.1	0.0			0.47453	0.44486	0.44687
		0.3	1	1	0.47911	0.45032	0.45227
		0.5			0.48194	0.45368	0.45560
		1			0.48832	0.46123	0.46307
0.5	0.1	0.3	0		1.73621	1.39627	1.41615
			0.5	1	0.75536	0.68516	0.68976
			1		0.47911	0.45032	0.45227
			2		0.27621	0.26652	0.26719
0.5	0.1	0.3	1	0	0.42773	0.40282	0.40450
				0.5	0.45530	0.42788	0.42973
				1	0.47911	0.45032	0.45227
				1.5	0.49926	0.47005	0.47204

The velocity ratio parameter λ and slip parameter δ also significantly influences the skin friction. When $\lambda < 1$, the ambient fluid moves faster than the stretching surface, pulling the slower fluid forward. This produces a positive shear stress in the flow direction, resulting in a positive skin friction coefficient. At $\lambda = 1$, the fluid and surface move at the same velocity, so no dragging occurs, and the skin friction becomes zero. For $\lambda > 1$, the fluid near the surface moves faster than the ambient fluid, creating shear stress opposite to the free stream and yielding a negative skin friction.

The slip parameter reduces skin friction by allowing the fluid to slide more easily over the surface. As δ increases, the velocity gradient at the wall decreases because the direct contact between fluid and surface is reduced. This lowers the wall shear stress, resulting in a decrease in the skin friction coefficient.

In contrast, the magnetic field parameter M increases skin friction. The Lorentz force produced by the magnetic field opposes the motion of the electrically conducting nanofluid, effectively enhancing the viscous resistance. This deceleration strengthens the interaction between the fluid and the surface, leading to higher wall shear stress and an increased skin friction coefficient.

Finally, increasing the nanoparticle volume fraction ϕ and suction parameter γ also raises the skin friction coefficient. Higher ϕ increases fluid density and viscosity, while stronger suction draws the fluid toward the wall, both contributing to enhanced wall shear effects.

Effect on Local Nusselt Number, $Nu_x(Re_x)^{-1/2}$

Table 6 shows the influence of the governing parameters on the local Nusselt number. Increasing the nanoparticle volume fraction ϕ enhances the heat transfer rate compared to the base fluid case ($\phi = 0$). This improvement occurs because the suspended nanoparticles increase the effective thermal conductivity of the nanofluid, allowing more efficient energy exchange between the solid particles and the base fluid.

Table 6

Values of $Nu_x(Re_x)^{-1/2}$ *for various values of the parameter*

		Variables				Nanoparticles	
λ	φ	M	δ	γ	Cu	Al_2O_3	TiO_2
0	0.1	0.3	1	1	6.95116	6.84209	6.79949
0.5					7.03306	6.94410	6.89795
1					7.11109	7.04020	6.99077
1.5					7.18570	7.13118	7.07870
0.5	0	0.3	1	1	6.92225	6.92225	6.92225
	0.05				6.97607	6.93087	6.90871
	0.1				7.03306	6.94410	6.89795
	0.2				7.16419	6.98678	6.88600
0.5	0.1	0.0	1	1	7.03013	6.94050	6.89449
		0.3			7.03306	6.94410	6.89795
		0.5			7.03485	6.94631	6.90006
		1			7.03888	6.95123	6.90480
0.5	0.1	0.3	0	1	6.80445	6.71657	6.67514
			0.5		6.98602	6.89119	6.84652
			1		7.03306	6.94410	6.89795
			2		7.06663	6.98413	6.93670
0.5	0.1	0.3	1	0	2.14415	2.09843	2.05651
				0.5	4.39739	4.33048	4.28596
				1	7.03306	6.94410	6.89795
				1.5	9.84683	9.73399	9.68445

Among the nanofluids considered, Cu nanofluid exhibits the highest heat transfer rate, followed by Al_2O_3 and TiO_2 nanofluids. This trend is primarily due to the higher thermal conductivity of Cu nanoparticles, which allows heat to be conducted more efficiently from the surface into the fluid, resulting in a higher local Nusselt number.

The magnetic field parameter M also increases the local Nusselt number for all nanofluids. The Lorentz force generated by the magnetic field suppresses fluid motion near the wall, reducing the momentum boundary layer thickness. A thinner thermal boundary layer produces a steeper temperature gradient at the surface, and since the local Nusselt number is proportional to the wall temperature gradient, the heat transfer rate is enhanced.

Similarly, increasing the suction parameter γ significantly improves the heat transfer. Suction removes heated fluid from the surface and replaces it with cooler fluid from the outer region. This continuous replacement accelerates the removal of thermal energy, producing a higher heat flux and increasing the local Nusselt number.

Finally, higher values of the velocity ratio parameter λ and slip parameter δ also contributes to an increase in the local Nusselt number. These parameters facilitate faster fluid motion near the surface, which enhances the heat transfer characteristics of the nanofluid flow.

Effect of Velocity Ratio, λ

The velocity ratio parameter $\lambda = a/b$ represents the ratio of the stretching surface velocity a to the ambient fluid velocity b. Figure 2(a) illustrates the effect of λ on the nanofluid velocity profile. When $\lambda = 0$, the stretching surface is stationary, so the fluid motion near the surface depends entirely on the slip parameter. For $0 < \lambda < 1$, the nanofluid velocity gradually increases toward the ambient fluid velocity. At $\lambda = 1$, where the surface and ambient velocities are equal ($a = b$), the velocity profile becomes uniform, showing no increase or decrease. When $\lambda > 1$, the velocity near the surface initially exceeds the ambient velocity but gradually decreases toward it.

Figure 2

The (a) velocity and (b) temperature profiles for different values of λ

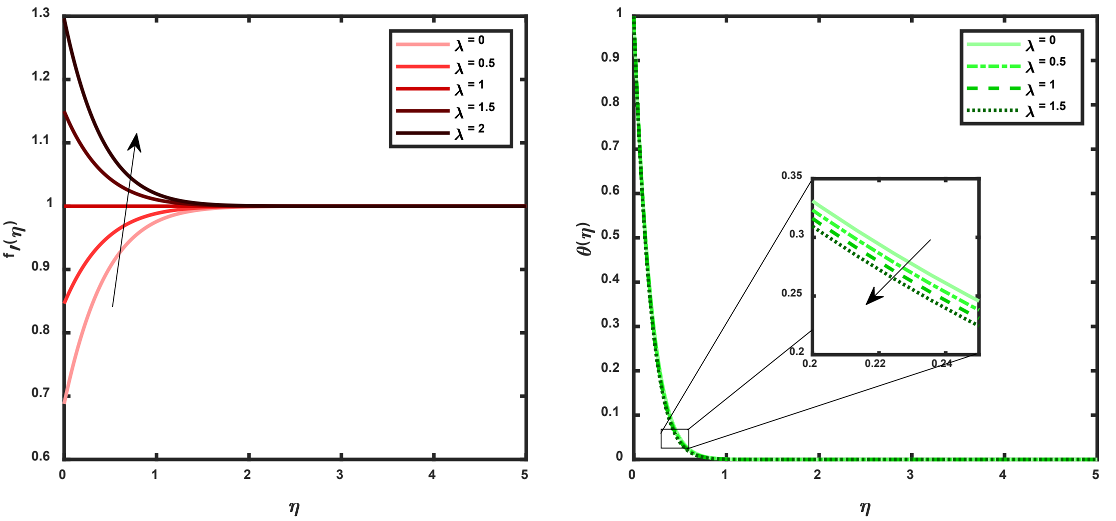

(a) (b)

Figure 2(b) shows the effect of λ on the temperature profile. Increasing λ slightly reduces the fluid temperature near the surface. This occurs because faster fluid spends less time in contact with the hot surface, absorbing less heat, while simultaneously carrying the warm fluid away and allowing cooler fluid to replace it. These combined effects lead to a thinner thermal boundary layer and a small decrease in temperature as λ increases.

Effect of Nanoparticle Volume Fraction (ϕ)

The nanoparticle volume fraction ϕ represents the concentration of Al_2O_3 nanoparticles in the base fluid. Figure 3(a) shows the effect of ϕ on the velocity profile. When a small fraction of nanoparticles is added ($0 < \phi \leq 0.05$), the nanofluid viscosity increases slightly, but the fluid can still move easily, resulting in a slight increase in velocity. However, as ϕ increases further ($0.05 < \phi \leq 0.2$), the viscosity rises significantly, making the fluid heavier and more resistant to motion, which causes the velocity profile to decrease.

Figure 3

The (a) velocity and (b) temperature profiles for different values of ϕ

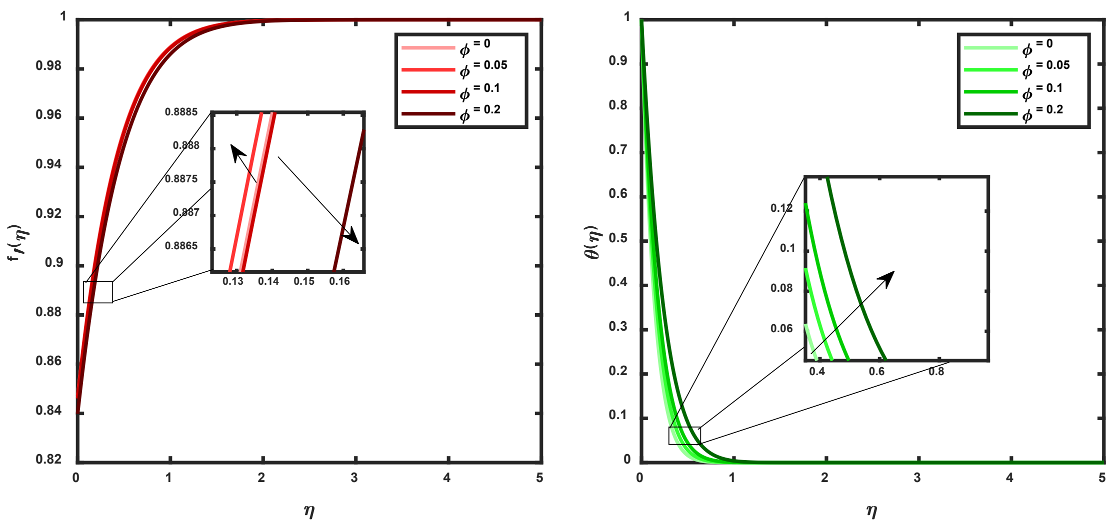

(a) (b)

Figure 3(b) illustrates the effect of ϕ on the temperature profile. Increasing the nanoparticle concentration enhances the thermal conductivity of the nanofluid, which improves heat transfer from the surface to the fluid. Consequently, the temperature within the boundary layer increases as ϕ rises.

Effect of Magnetic Field, M

Figure 4(a) illustrates the effect of the magnetic field parameter M on the velocity profile. When $M = 0$, no magnetic field is applied, and the nanofluid behaves as a normal electrically conducting fluid. As M increases, the applied magnetic field generates a Lorentz force that acts on the moving electric charges in the fluid, stabilizing the motion of the nanofluid and aligning the movement of nanoparticles. This reduces the random motion of nanoparticles, allowing the fluid to move more smoothly, which results in an increase in velocity near the surface.

Figure 4

The (a) velocity and (b) temperature profiles for different values of M

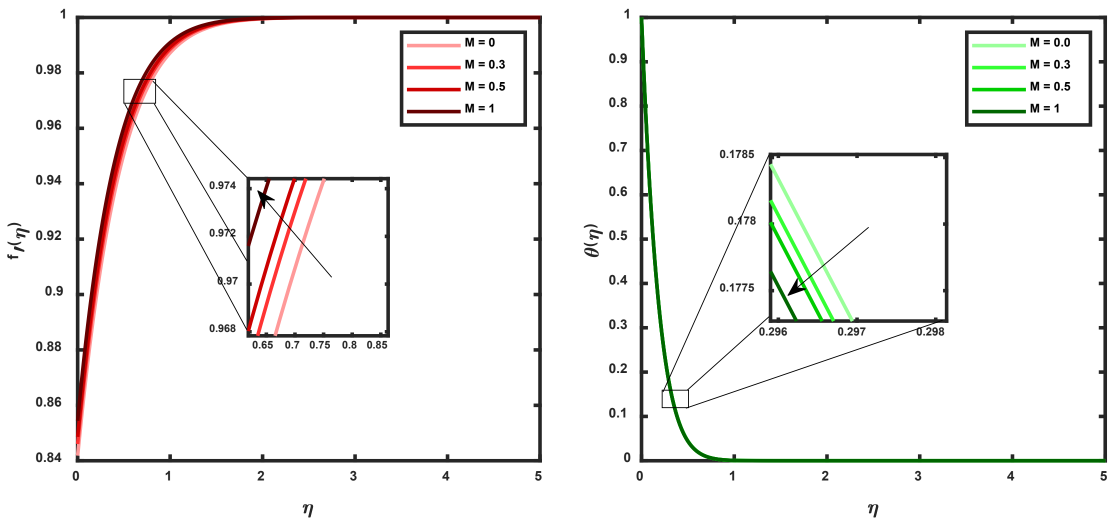

(a) (b)

Figure 4(b) shows the corresponding temperature profiles. The higher fluid velocity, combined with the suction effect, removes hot fluid from the wall more quickly, reducing the residence time of heat near the surface. At the same time, the stabilized nanofluid enhances the smooth transport of heat, leading to an overall decrease in the temperature profile within the boundary layer.

Effect of Velocity Slip, δ

Figure 5(a) illustrates the effect of the slip parameter δ on the velocity profile. As δ increases, the fluid experiences less resistance at the wall and can slide more smoothly along the surface. In contrast, under the no-slip condition ($\delta = 0$), the fluid at the wall matches the wall velocity, limiting motion. With higher δ, the wall offers reduced friction, allowing the fluid to move faster, which increases the velocity profile near the surface.

Figure 5

The (a) velocity and (b) temperature profiles for different values of δ

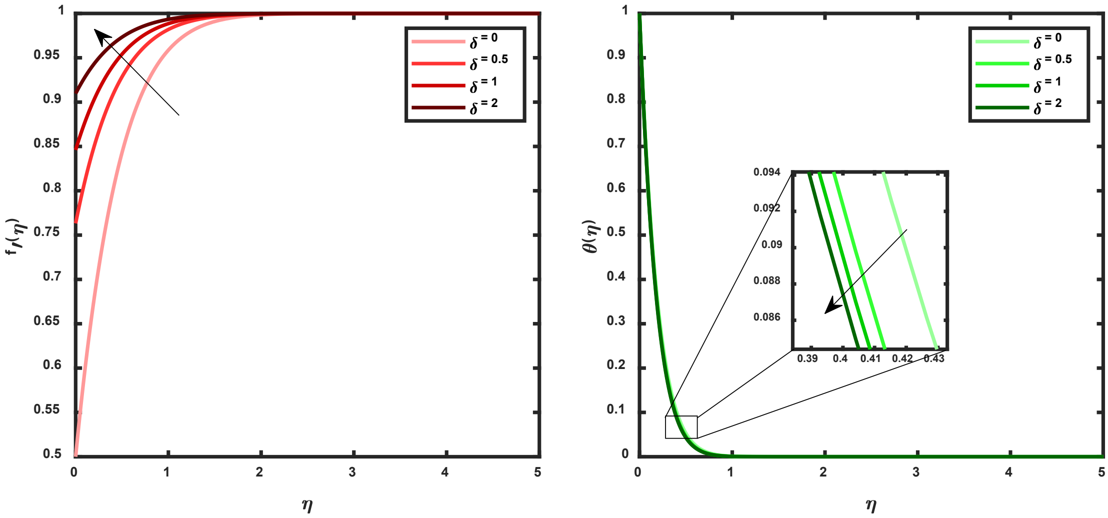

(a) (b)

Figure 5(b) shows the corresponding temperature profiles. As the slip parameter δ increases, the temperature decreases. This occurs for two main reasons. First, the reduced friction at the wall lowers the amount of heat generated from viscous effects. Second, the faster-moving fluid carries heat away more quickly, so the fluid particles remain near the hot surface for a shorter time. Because the fluid is exposed to the surface for less time, less heat is absorbed, and the thermal boundary layer becomes thinner. These combined effects lead to a lower temperature profile as the slip parameter increases.

Effect of Suction, γ

Figure 6(a) shows the effect of the suction parameter γ on the velocity profile. As γ increases, the thick, slow-moving fluid near the wall is removed, which reduces the boundary layer thickness. With a thinner boundary layer, the fluid near the wall experiences less resistance, allowing the faster-moving fluid from the outer region to move toward the surface. This results in an increase in the velocity profile near the wall.

Figure 6

The (a) velocity and (b) temperature profiles for different values of γ

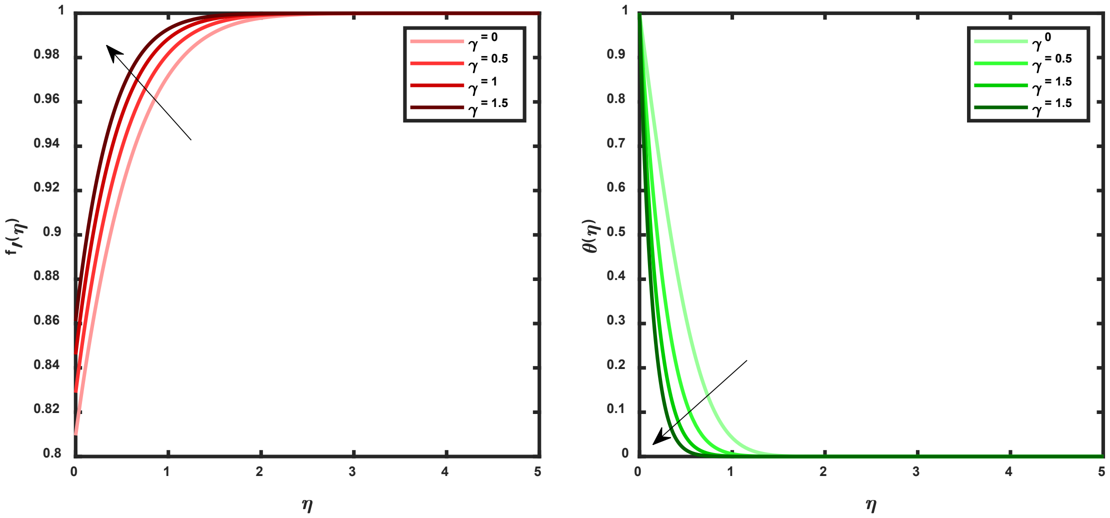

(a) (b)

Figure 6(b) shows the corresponding temperature profiles. Increasing the suction parameter γ decreases the temperature profile. This occurs because suction removes heated fluid from the surface, allowing cooler fluid from the outer region to replace it. As the heated fluid is carried away, less heat remains trapped near the wall, causing the thermal boundary layer to become thinner. Consequently, the temperature of the fluid near the surface decreases as the suction parameter increases.

CONCLUSION

This study analyzed the magnetohydrodynamic (MHD) flow of water-based nanofluids over a stretching surface, considering the effects of magnetic field, suction, velocity slip, velocity ratio, and nanoparticle volume fraction on flow and heat transfer.

The analysis shows that an increased magnetic field enhances wall shear and heat transfer by stabilizing the fluid motion and reducing boundary layer thickness. Suction accelerates fluid near the wall and removes heat efficiently, raising the local Nusselt number. Higher slip allows the fluid to move more easily along the surface, increasing velocity while slightly lowering the temperature near the wall. The velocity ratio governs the direction and magnitude of shear stress, and higher nanoparticle volume fraction improves heat transfer through enhanced thermal conductivity, although excessive addition may reduce velocity due to increased viscosity.

The comparison between different nanoparticles shows that copper produces the highest wall shear stress and heat transfer rate. However, the results also indicate that aluminium oxide offers a more practical option for engineering applications because it provides reliable heat transfer performance while maintaining good stability, corrosion resistance, and lower cost. This finding highlights the importance of balancing thermal performance with practical considerations when selecting nanoparticles for nanofluid systems.

Several limitations should be acknowledged. The present analysis considers steady, laminar, two-dimensional flow with constant thermophysical properties and a fixed Prandtl number. The model also assumes a uniform nanoparticle distribution and does not account for particle agglomeration, sedimentation, or temperature-dependent properties that may occur in real systems. Therefore, the results are most applicable to idealized conditions and should be interpreted with these constraints in mind.

Future studies may extend the present model by incorporating temperature-dependent properties, hybrid nanofluids, or unsteady flow conditions. Additional work could also examine three-dimensional configurations, different base fluids, or more complex boundary conditions that better represent practical thermal systems. Such extensions would improve the predictive capability of the model and provide deeper insight into the application of MHD nanofluids in advanced heat transfer technologies.

ACKNOWLEDGEMENT

The authors have no conflicts of interest to declare. This research received no specific grant from any funding agency in the public, commercial, or not-for-profit sectors.

REFERENCES

Alabdulhadi, S., Ishak, A., Waini, I., & Ahmed, S. (2023). Non-Unique Solutions of Magnetohydrodynamic Stagnation Flow of a Nanofluid towards a Shrinking Sheet Using the Solar Radiation Effect. *Micromachines*, *14*(3), 565. https://doi.org/10.3390/mi14030565

Alias, N. N., Rosali, H., Bachok @ Lati, N., & Ioan Pop. (2025). MHD Stagnation Point Flow over a Stretching/Shrinking Sheet in Nanofluid with Suction Effect. *Journal of Science and Mathematics Letters*, *13*(1), 51-60. https://doi.org/10.37134/jsml.vol13.1.6.2025

Choi, S. U. S., & Eastman, J. A. (1995). *Enhancing thermal conductivity of fluids with nanoparticles*. *66*. https://www.researchgate.net/publication/236353373_Enhancing_thermal_conductivity_of_fluids_with_nanoparticles

Emam, T. G., Fathy, M., Alharbi, M. H., & Abdelgaber, K. M. (2025). Significance of thermal radiation and suction/injection on flow and heat transfer of various nanofluids along expandable stretching horizontal cylinder. *Boundary Value Problems*, *2025*(1). https://doi.org/10.1186/s13661-025-02010-0

Hussein, A. A., Auda, A. C., Showard, A. F., & Dawood, H. I. (2025). Heat Transfer Enhancement by utilizing Al2O3-Water Nanofluid in a Coiled Agitated Vessel. *Case Studies in Thermal Engineering*, *66*, 105740–105740. https://doi.org/10.1016/j.csite.2024.105740

Jagadish V. Tawade, P. P. . (2022). Effect of Thermal and Solutal Slip on Stagnation Point Flow of Nanofluid over a Stretching Sheet . *Mathematical Statistician and Engineering Applications*, *71*(4), 12698–12713. https://doi.org/10.17762/msea.v71i4.2483

Japili, N., Rosali, H., & Bachok, N. (2022). *Slip effect on stagnation point flow and heat transfer over a shrinking/stretching sheet in a porous medium with suction/injection***.** *Journal of Advanced*

Research in Fluid Mechanics and Thermal Sciences, 90(2), 73–89. https://doi.org/10.37934/arfmts.90.2.7389

Joyce, M. I., Kandasamy, J., & Sivasankaran Sivanandam. (2023). Entropy Generation of Cu–Al2O3/Water Flow with Convective Boundary Conditions through a Porous Stretching Sheet with Slip Effect, Joule Heating and Chemical Reaction. *Mathematical and Computational Applications*, *28*(1), 18–18. https://doi.org/10.3390/mca28010018

Karimdoost Yasuri, A. and Soleimani, E. (2021). An Experimental Study on the Simultaneous Effect of Nanofluid and Tube Insert on the Thermal Performance of an Automobile Cooling System. *Journal of Applied Fluid Mechanics*, *14*(5), 1559-1566. doi: 10.47176/jafm.14.05.32421

Khan, A. A., Zaimi, K., & Teh, Y. Y. (2022). Unsteady MHD stagnation point flow of Al_2O_3–Cu/H_2O hybrid nanofluid past a convectively heated permeable stretching/shrinking sheet with suction/injection. *Journal of Advanced Research in Fluid Mechanics and Thermal Sciences, 96*(1), 96–114. https://doi.org/10.37934/arfmts.96.1.96114

Khan, M. N., & Nadeem, S. (2021). MHD stagnation point flow of a Maxwell nanofluid over a shrinking sheet (multiple solution). *Heat Transfer*, *50*(5), 4729–4743. https://doi.org/10.1002/htj.22098

Khashi'ie, N. S., Wahi, N., Arifin, N. M., Ghani, A. A., & Hamzah, K. B. (2022). Effect of suction on the MHD flow in a doubly-stratified micropolar fluid over a shrinking sheet. *Mathematical Modeling and Computing*, *9*(1), 92–100. https://doi.org/10.23939/mmc2022.01.092

Nor, N., Bachok, N., Pop, N. I., Arifin, N., & Rosali, H. (2022*). Stability solution of unsteady stagnation-point flow and heat transfer over a stretching/shrinking sheet in nanofluid with slip velocity effect***.** *CFD Letters, 14*(1), 66–86. https://doi.org/10.37934/cfdl.14.1.6686

Othman, M. N., Jedi, A., & Bakar, N. A. A. (2021). MHD Stagnation Point on Nanofluid Flow and Heat Transfer of Carbon Nanotube over a Shrinking Surface with Heat Sink Effect. *Molecules*, *26*(24), 7441. https://doi.org/10.3390/molecules26247441

Oyekunle, T. L., Mojeed Taiwo Akolade, Agunbiade, S. A., & Adeniran, P. O. (2024). *MHD Stagnation Point Flow of Nanofluid with Buoyancy Effect Through a Porous Shrinking Sheet*. *19*(1), 1–15. https://www.researchgate.net/publication/381734106_MHD_Stagnation_Point_Flow_of_Nanofluid_with_Buoyancy_Effect_Through_a_Porous_Shrinking_Sheet

Raza Shah Naqvi, S. M., Farooq, U., Waqas, H., Muhammad, T., & Alshehri, A. (2022). Inspection of thermal jump conditions on nanofluids with nanoparticles and multiple slip effects. *Scientific Reports*, *12*(1). https://doi.org/10.1038/s41598-022-07655-w

Safiei, W., Rahman, Md. M., Hadi, M. A., Azmi, W. H., & Arifin, M. N. (2020). Experimental Investigation on Preparation and Stability of Al2O3 Nanofluid In Deionized Water and Ethylene Glycol. *Journal of Advanced Research in Fluid Mechanics and Thermal Sciences*, *77*(2), 47–62. https://doi.org/10.37934/arfmts.77.2.4762

Yashkun, U., Zaimi, K., Abu Bakar, N. A., & Ferdows, M. (2020). Nanofluid stagnation-point flow using Tiwari and Das model over a stretching/shrinking sheet with suction and slip effects.

Journal of Advanced Research in Fluid Mechanics and Thermal Sciences, 70(1), 62–76. https://doi.org/10.37934/arfmts.70.1.6276

Zainal, N. A., Nazar, R., Naganthran, K., & Pop, I. (2022). *Unsteady separated stagnation-point flow past a moving plate with suction effect in hybrid nanofluid***.** *Mathematics, 10*(11), 1933. https://doi.org/10.3390/math10111933

Zhang, X.-H., Abidi, A., Ahmed, A. E.-S., Khan, M. R., El-Shorbagy, M. A., Shutaywi, M., Issakhov, A., & Galal, A. M. (2021). MHD stagnation point flow of nanofluid over a curved stretching/shrinking surface subject to the influence of Joule heating and convective condition. *Case Studies in Thermal Engineering*, *26*, 101184. https://doi.org/10.1016/j.csite.2021.101184

Zheng, D., Wang, J., Pang, Y., Chen, Z., & Sunden, B. (2020). Heat transfer performance and friction factor of various nanofluids in a double-tube counter flow heat exchanger. *Thermal Science*, *24*(6 Part A), 3601–3612. https://doi.org/10.2298/tsci200323280z